Graduate School of Oceanography Faculty
Publications

Graduate School of Oceanography

2002

Equatorial Pacific Subsurface Countercurrents: A Model–Data Comparison in Stream Coordinates

Kathleen A. Donohue
University of Rhode Island, kdonohue@uri.edu

Eric Firing

G. Dail Rowe

Akio Ishida

Humio Mitsudera

Follow this and additional works at: https://digitalcommons.uri.edu/gsofacpubs

Equatorial Pacific Subsurface Countercurrents: A Model–Data Comparison in Stream Coordinates

NOTES AND CORRESPONDENCE

Equatorial Pacific Subsurface Countercurrents: A Model–Data Comparison in Stream Coordinates*

KATHLEEN A. DONOHUE

University of Rhode Island, Narragansett, Rhode Island

ERIC FIRING

University of Hawaii, Honolulu, Hawaii

G. DAIL ROWE

Accurate Environmental Forecasting Inc., Narragansett, Rhode Island

AKIO ISHIDA

Japan Marine Science and Technology Center, Yokosuka, Japan

HUMIO MITSUDERA

International Pacific Research Center, University of Hawaii, Honolulu, Hawaii

ABSTRACT

An isopycnal stream-coordinate analysis of velocity, transport, and potential vorticity (PV), recently applied to observations of the subsurface countercurrents (SCCs) in the equatorial Pacific Ocean, is applied here to the SCCs in a numerical general ocean circulation model, run by the Japan Marine Science and Technology Center (JAMSTEC). Each observed SCC core separates regions of nearly uniform potential vorticity: low on the equatorward side, high on the poleward side. Similar low-PV pools are found in the model, but the high-PV region poleward of the southern SCC is missing. The potential vorticity gradient in each core is weaker in the model than in observations, and relative vorticity plays only a minor role in the model. Its unusually high vertical resolution, with 55 levels, together with its weak lateral dissipation may be key factors in the JAMSTEC model's ability to simulate SCCs.

1. Introduction

The Pacific equatorial subsurface countercurrents (SCCs) are narrow eastward jets found a few degrees on either side of the equator, below the sharp equatorial thermocline (Fig. 1) (Tsuchiya 1975). Johnson and Moore (1997) and Johnson and McPhaden (1999) pro-

vide a comprehensive description of the SCCs using all available hydrographic data in the tropical Pacific. Combined with the hydrographic sections and analyzed in stream coordinates, shipboard acoustic Doppler current profiler (ADCP) sections show the SCCs with higher spatial resolution than in prior studies (Rowe et al. 2000). Each SCC core has a potential vorticity front about 40 km wide, separating regions of nearly constant potential vorticity. Relative vorticity contributes significantly to the sharpness of the front.

Two recent theoretical studies of the SCCs are inconsistent. Johnson and Moore (1997) modeled them as inertial jets; the observed downstream divergence of the jet cores from the equator is then a consequence of the mean tilt of the equatorial thermocline, upward to the east, that forms their upper boundary. Their downstream

acceleration and reduction in width are attributed to the role of relative vorticity in the potential vorticity balance. Marin et al. (2000) suggest that the SCCs are the ocean analog of the atmospheric Hadley cells and associated jet streams. Their two-dimensional model produces subpycnocline eastward jets separated by an equatorial region of homogenized low potential vorticity. Circulation in the vertical–meridional plane is essential to their model, but absent from the Johnson and Moore (1997) model.

An even more recent study of the SCCs is generally consistent with the Johnson and Moore (1997) model, but is much more complete. Using analytic and simplified numerical models, McCreary et al. (2002, hereafter MLY) describe the SCCs as jets that are forced by upwelling along the South American coast and in the eastern Pacific ITCZ, possibly augmented by eddy momentum flux convergence. They flow along fronts that form at the convergence of long Rossby wave characteristics.

The SCCs have not figured prominently in analyses of numerical general circulation models, although their Atlantic counterparts, the north and south equatorial undercurrents, have been described in a high-resolution Atlantic model (Schott and Böning 1991). In the Pacific, SCCs are identifiable in a 3-yr mean meridional section of zonal velocity at 150°W from the Parallel Ocean Program (POP) model (Maltrud et al. 1998, their Fig. 6).

The recent Japan Marine Science and Technology Center (JAMSTEC) high-resolution general circulation model (Ishida et al. 1998b) produces SCCs with many features in common with observations (Ishida et al. 1998a). For example, Ishida et al. (1998a) show that the density of the SCCs decreases downstream in the model as in the ocean. The modeled SCCs do not show the observed downstream divergence from the equator, and the velocity and transport of model SCCs are particularly weak in the west compared to observations (Ishida et al. 1998a) (Fig. 1).

The JAMSTEC model SCCs resemble the observations sufficiently to warrant closer examination, in the hope that both the model's shortcomings and its successes may provide insight into SCC dynamics in the ocean. A comprehensive isopycnal analysis of the model SCCs is provided by Ishida et al. (2001, unpublished manuscript). The purpose of this note is to contribute to the JAMSTEC model analysis with a comparison to observations, using the Rowe et al. (2000) methodology.

2. Model and methods

The JAMSTEC global circulation model is based on the Modular Ocean Model version 2 (Pacanowski 1995). The model domain is 75°S–75°N, with no Arctic Ocean. Topography is based on 5-min gridded earth topography (ETOPO5) data. Horizontal grid spacing for each variable is 0.25°. With its 55 levels, the JAMSTEC model has unusually high vertical resolution for a global GCM.

The grid spacing increases smoothly from 10 m at the surface through 50 m near 600 m, reaching 700 m at the bottom (6000 m).

The model is spun up from a state of rest with temperature and salinity initialized to the annual average Levitus (1982) climatology. Heat and freshwater fluxes are established by linear relaxation of temperature and salinity in the first model level toward Levitus climatology. The restoring timescale is 6 days. Wind forcing is from the Hellerman and Rosenstein (1983) wind stress climatology. The first two years of model spinup use annually averaged climatologies for surface boundary conditions and a harmonic operator for the horizontal dissipation mechanism. In all subsequent years the model is driven by monthly climatologies, and the horizontal dissipation is via a biharmonic operator with coefficient -1×10^{-19} cm^4 s^{-1} for momentum and tracers. The vertical dissipation is handled through the Pacanowski and Philander (1981) formulation. Below 2000 m, tracers are restored to Levitus (1982) climatology with a 2-yr timescale. In this note we describe the results from year 20. Model output is subsampled every 5 days.

Velocity structure, transport, and potential vorticity (PV) of the SCCs were determined for layers centered on neutral densities, γ, (Jackett and McDougall 1997); PV was estimated as

$$\frac{f - \partial u/\partial y}{h}. \quad (1)$$

The term "relative PV" denotes the contribution of relative vorticity to total PV:

$$-\frac{\partial u}{\partial y} \bigg/ h. \quad (2)$$

All quantities are calculated for each model snapshot and averaged in stream coordinates centered on each SCC velocity core. The term "core" denotes the location of the zonal velocity maximum, either of the entire current or within a specified depth or density range. The core latitude was initially chosen subjectively by inspection of the zonal velocity as a function of latitude and depth, and then refined by finding the maximum in the surrounding 1° by 200 m rectangle. The core latitude in a given neutral density range was determined by using the initial core latitude from the latitude–depth analysis and finding the maximum within a 1° range. When a velocity core could not be identified unambiguously, the snapshot was excluded from the average. Model sections were extracted every 5° longitude between 140°E and 100°W. For the northern SCC (NSCC), a core was identified in 95% of the samples between 140°E and 100°W. The Southern Hemisphere SCCs appear east of 155°E; between 155°E and 100°W, the primary Southern Hemisphere core (SSCC) was identified in 80% of the sections. The secondary core, located south of the primary core, was found in 65% of the samples. This selection procedure inevitably bi-
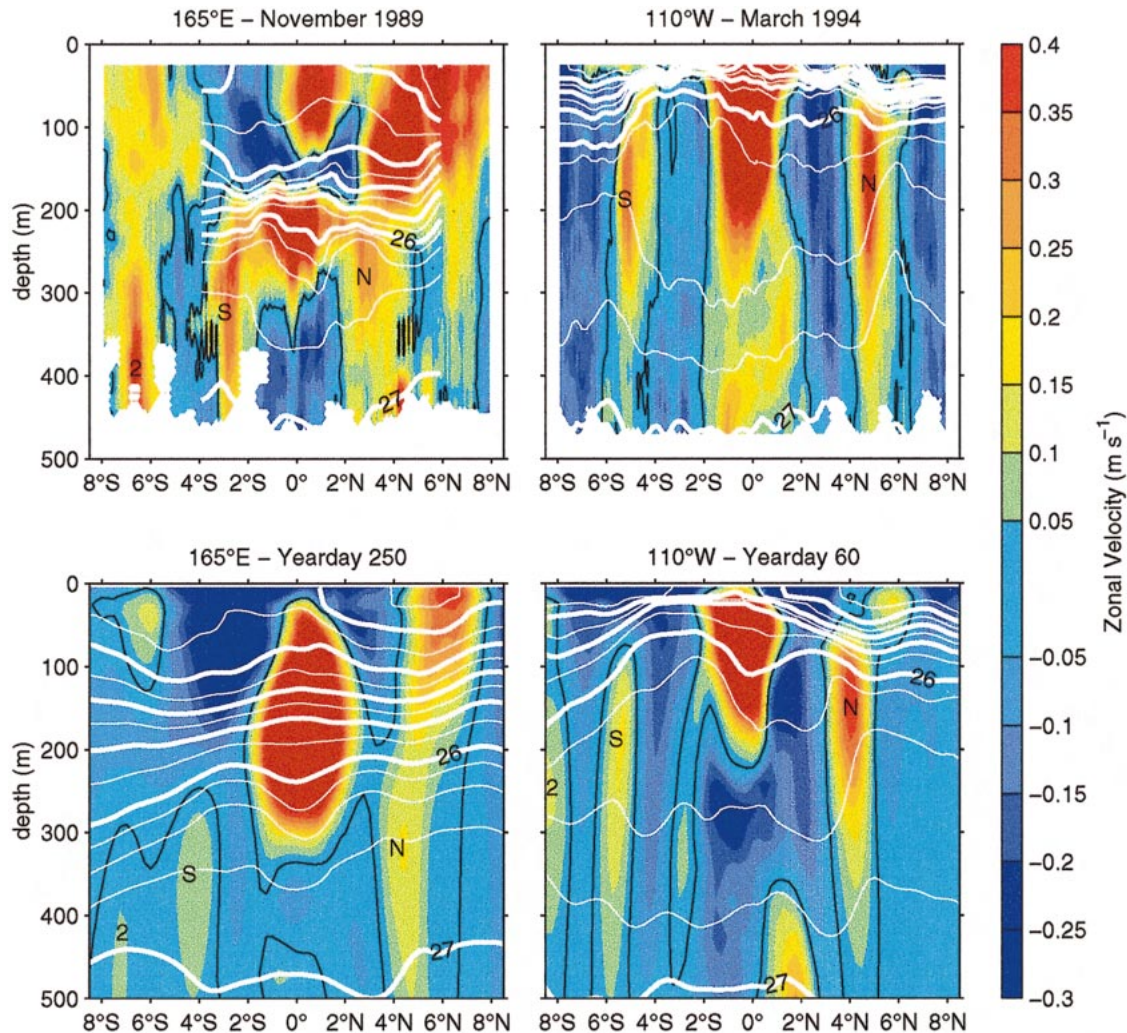
FIG. 1. Typical synoptic sections of zonal velocity and neutral density showing the SCCs in the western Pacific (left) and in the eastern Pacific (right) from observations (upper panels) and from the JAMSTEC model (lower panels). The zero zonal velocity contour is black. Neutral density is contoured in white at intervals of 0.5 kg m^{-3} for $\gamma < 26.0$ and 0.25 kg m^{-3} for $\gamma > 26.0$, and with thick contours at integer values. Observations show that as the SCCs (labeled **S** for the southern jet and **N** for the northern jet) flow eastward they rise with the equatorial thermocline and diverge from the equator. Modeled SCCs exhibit downstream lightening but not divergence (Ishida et al. 1998a,b). Modeled SCCs are weaker than observed, especially in the western Pacific (Ishida et al. 1998a,b). The secondary southern SCC (labeled 2) appears in both model sections but is only apparent in the western Pacific observation, 165°E section. The secondary SSCC may have been beyond the southern end of the observed 110°W section.

ases the results, but we know of no way to conduct the model stream-coordinate analysis without this consequence.

3. Comparison

a. Core position

As they flow from west to east, the SCC cores diverge from the equator and decrease in density; the core depths rise to the east more steeply than the isopycnal surfaces. The modeled primary SCC core positions determined from annual mean fields have been discussed by Ishida et al. (1998a, their Fig. 4). Consistent with their findings, our stream-coordinate analysis shows that the modeled

primary SCC cores fail to diverge from the equator (Fig. 2). The modeled secondary SCC core behavior, however, matches the observations in latitude and density.

The primary SCC cores are about 3° from the equator in the western Pacific and reach maximum latitudes of 6° near 125°W (Rowe et al. 2000). In contrast, the model SCC core latitudes are nearly constant across the basin, at 4°N for the NSCC and 4.5°S for the SSCC. West of 140°W, observed and modeled primary SCC core densities are similar, decreasing eastward by about 0.1 kg m^{-3} per 20° longitude. East of 140°W, the modeled cores continue to lighten at the same rate, but the observed cores are nearly isopycnal.

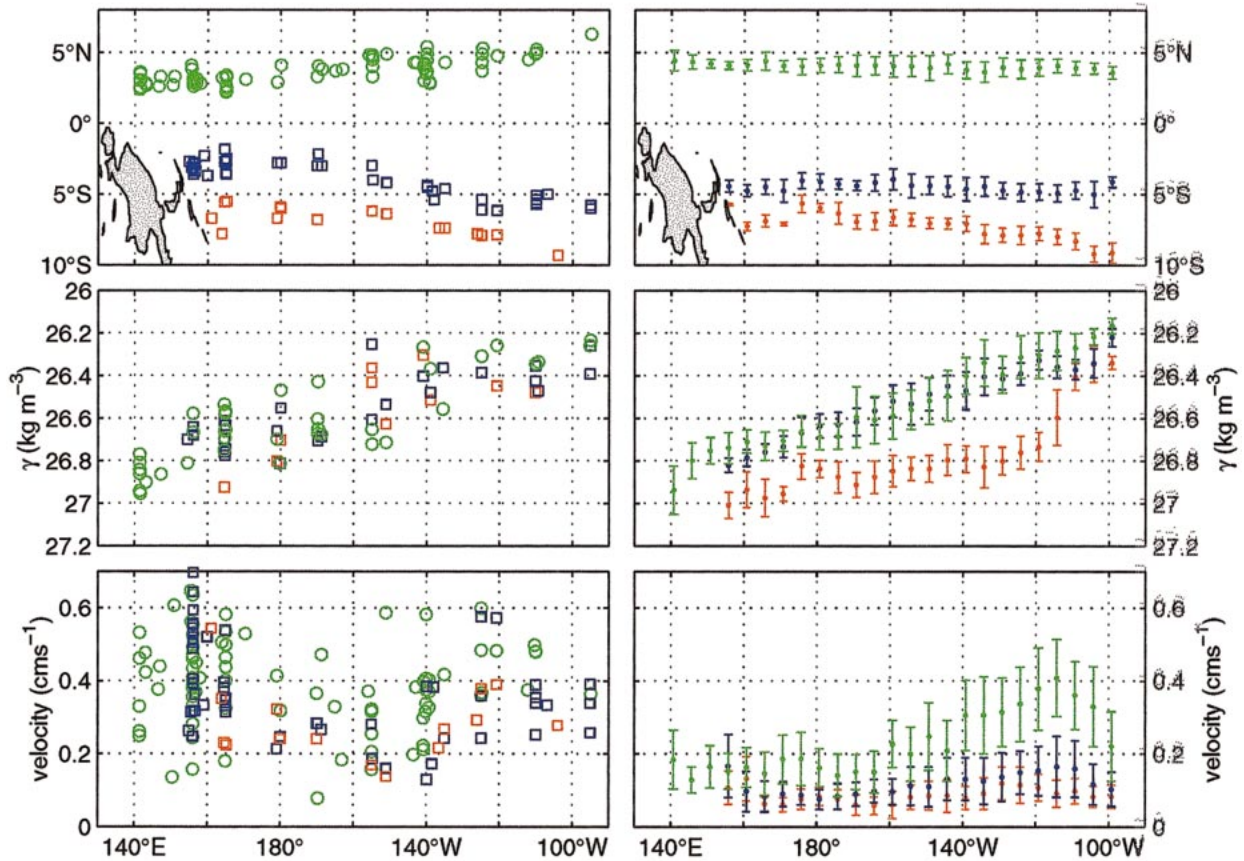The modeled secondary SSCC core latitude matches

FIG. 2. Core positions (top, and middle panels) and velocities (bottom) of the SCCs. Bars on model show plus/minus one standard deviation. Observations (left panels) from Rowe et al. (2000) are shown with large solid circles and squares. The model (right panels) reproduces the progressive eastward lightening but not the equatorial divergence of the primary SCC cores. Maximum core velocity in the model NSCC is found near 115°W. Core positions revealed by the stream-coordinate analysis are consistent with the previous findings of Ishida et al. (1998a).
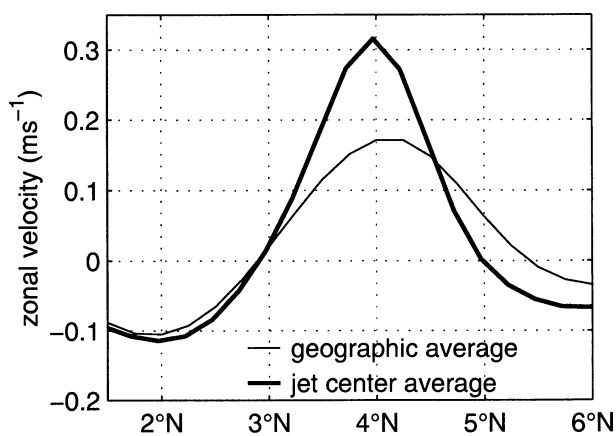

FIG. 3. Zonal component of model NSCC averaged in the 26.3–26.5 kg m^{-3} neutral density layer. Eight sections between 140° and 110°W are averaged in geographical coordinates (light line) and in stream coordinates (heavy line). The geographical average decreases the magnitude and broadens the jet. The stream-coordinate profile is aligned with its core at the mean latitude of the individual section cores.

the observations remarkably well. It is near 7°S in the western and central Pacific, and gradually shifts poleward to the east in the eastern Pacific. The match in core density is not as uniform; the modeled secondary SSCC core neutral density in the western Pacific is near 26.95 kg m^{-3} as observed, and lightens to about 26.4 kg m^{-3} in the east, but the downstream reduction in core density occurs primarily in the west in the observations and in the east in the model. Observed secondary SSCC core depths in the west and central basin are biased shallow by the limited depth range of the ADCP, however.

b. Velocity structure

In the model as in the observations, stream-coordinate averaging yields narrower and stronger mean SCC profiles compared to averaging in geographical coordinates (Fig. 3); the core latitude varies temporally over a range of roughly 2°, the width of the jet.

The modeled SCC meridional profiles of zonal velocity have maximum speeds roughly half the observed maxima and lack the nearly triangly shape character-
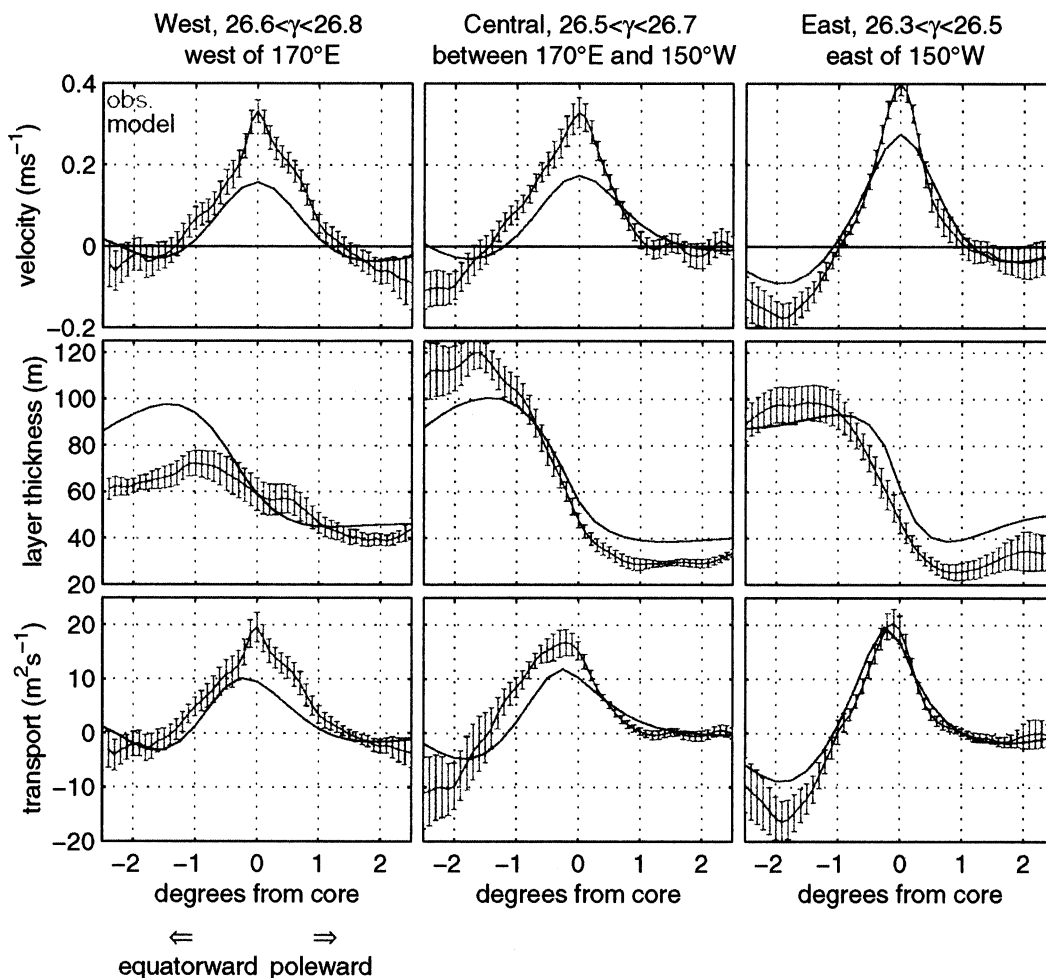
FIG. 4. Velocity, thickness, and transport of the NSCC at core neutral density layers averaged in three longitude regions from the model (solid lines) and observations (lines with bars), from Rowe et al. (2000). Bars show one standard error. The abcissa in all panels is degrees latitude from the current core, positive to the north. Model NSCC velocities are much weaker than observations (upper panels). Layer thickness is larger on the equatorward side of all NSCCs (middle panels). Westward flow exists equatorward of model and observed NSCC.

istic of the observations, but the overall jet widths differ little between model and observations, particularly in the NSCC (Figs. 4, 5). The 0.25° grid spacing in the model cannot resolve the sharp velocity peak observed at the core. The differences in velocity profile between the model and the observations are more pronounced in the SSCC, and especially in the secondary SSCC, than in the NSCC; the modeled secondary SSCC is about twice as wide as observed.

Westward flow along the flanks of the SCCs is present on the equatorward side of both model SCCs and on the poleward side of the northern SCC (Figs. 4, 5). Westward flow observed south of the SSCC, and on both flanks of the secondary SSCC, is absent from the model (Fig. 6).

In the model as in observations, the mean meridional velocity component (v) is minuscule compared to the fluctuations. Using the stream-coordinate averaging of the Rowe et al. (2000) shipboard ADCP sections (Fig.

7), we find a few places where the mean v exceeds its standard error, but no convincing or consistent pattern; many more sections would be required for a useful estimate of the mean. The model is of course much better sampled. Although we have not made a detailed comparison with other observations, inspection of the model v on the equator versus v measured by the equatorial Tropical Atmosphere–Ocean (TAO) moorings (Mc-Phaden et al. 1998) suggests that the model v field on the equator, at least, is reasonable; variability from tropical instability waves is similar to what was observed during the mild La Niña of 1998–99. The standard deviation of v in the model, averaged in stream coordinates and in the core density layer, increases from about 5 cm s^{-1} in the west to 10–20 cm s^{-1} in the east, with the largest values at the core latitude in the NSCC (Fig. 8). The mean v is less than 1 cm s^{-1} in magnitude almost everywhere, and less than 0.5 cm s^{-1} throughout four of the six regions in Fig. 8. Means and standard devi-
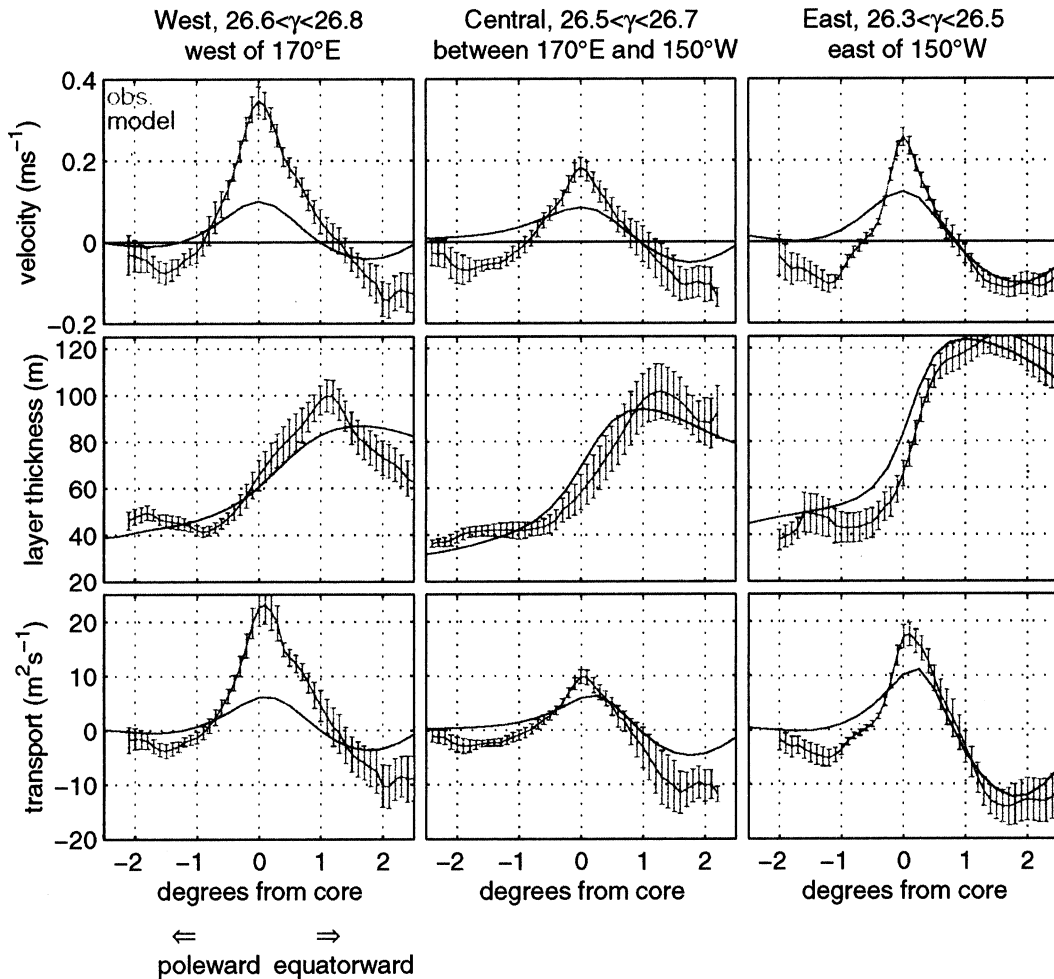
FIG. 5. Same as Fig. 4 but for the SSCC. Velocities and transports are much weaker compared to observations from Rowe et al. (2000), particularly in the west. Westward flow exists equatorward of model and observed SSCC. Weak westward flow poleward of the SSCC is present in the observations but not in the model.

ations for layers 0.2 and 0.4 kg m^{-3} above and below the core were nearly identical (not shown). We conclude that any true mean in the model v near the SCCs is likely to be no more than 0.5 cm s^{-1} in magnitude, and cannot be measured in our sample of model output.

c. Layer thickness and transport

The observed equatorward increase in layer thickness across each primary SCC core is also found in the model; the largest discrepancy is in the western NSCC, where the observed layer thickness jump is smaller than in the model, and also smaller than at other locations (Figs. 4, 5).

SCC transport per unit width is weaker in the model than in observations except in the eastern NSCC, where a slightly larger model layer thickness in the core compensates for the weaker modeled velocities. The flanking westward transport per unit width is also weaker in the model, except on the equatorward side of the eastern

SSCC, where layer thickness and velocity are nearly identical between the model and observations.

The model shows the observed downstream decrease in density of the transport core (Fig. 9), as expected from the similar downstream lightening of the velocity core (Fig. 2).

Although the maximum velocities in the model SCCs are weaker than observed, the mean transport of each SCC in the model (Fig. 9) is remarkably similar to estimates from observations (Rowe et al. 2000, their Table 2). The model NSCC transports 7–8 ($\times$ 10^6 m^3 s^{-1}) from 141°E to 144°W, increases to 11 $\times$ 10^6 m^3 s^{-1} at 119°W, and drops to 5 $\times$ 10^6 m^3 s^{-1} at 99°W. The model primary SSCC transports 3–4 ($\times$ 10^6 m^3 s^{-1}) from 166°E to 119°W, and 2 $\times$ 10^6 m^3 s^{-1} at 99°W. The model secondary SSCC transports 4 $\times$ 10^6 m^3 s^{-1} at 166°E, 3 $\times$ 10^6 m^3 s^{-1} at 169°W, and 5 $\times$ 10^6 m^3 s^{-1} at all sampled longitudes east of 169°W. Transport estimates from observations are not as well resolved as a function of longitude and vary considerably from one
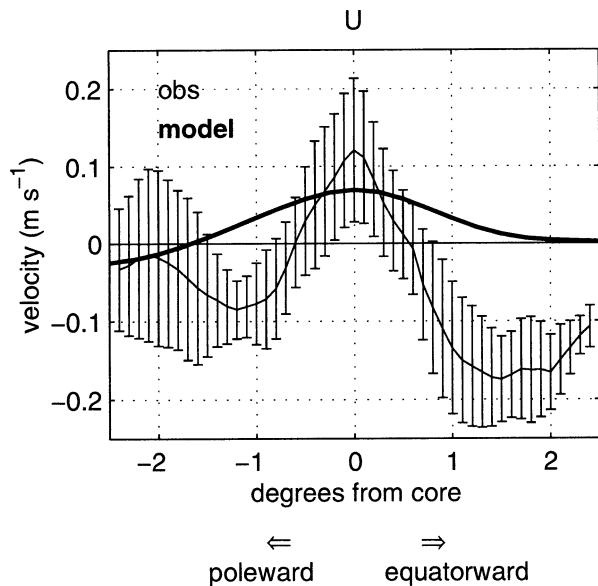
FIG. 6. Stream-coordinate comparisons of the secondary SSCC zonal velocity structure of the model (heavy line) and observations from Rowe et al. (2000) (light line) in neutral density layer 26.5–26.7 kg m^{-3} for longitudes between 180° and 140°W. The model SSCC is much weaker and broader than observed. The error bars show one standard error of the observed mean.

study to another, but the primary SCC transports tend to be larger than in the model by up to a factor of 2 in the west and nearly identical in the central and eastern regions. Observations indicate that the primary SSCC

transport in the central Pacific is smaller than in the west, but this is not seen in the model.

The secondary SSCC is poorly sampled by observations, and we are aware of no prior estimate of its transport. Figure 6 suggests that the greater width of the secondary SSCC in the model compared to observations may overcompensate for the weaker peak velocity in the model, so that the transport in the model may exceed that in the ocean; in any event, it is interesting that in the model the transport of the secondary SSCC exceeds that of the primary SSCC. Our estimate is probably biased high, however, by our exclusion of sections in which a core was not identified.

d. Potential vorticity

The observed SCC cores separate regions of nearly uniform PV: low on the equatorward side, high on the poleward side (Figs. 10, 11). PV is nearly a step function of distance from the SCC core due to the rapid reversal of relative PV (Rowe et al. 2000). The contribution of relative PV is smaller in the model, and the PV gradient at the core is much weaker than observed. The model produces nearly uniform low PV in the region of westward flow equatorward of the primary SCCs, as observed, but the match is not as good on the poleward sides. South of the SSCC, there is no uniform PV region in the model at all; the model PV gradient is only slightly smaller there than at the core. North of the NSCC, the model PV increases only slowly with latitude in the western and central regions, and it decreases with lat-
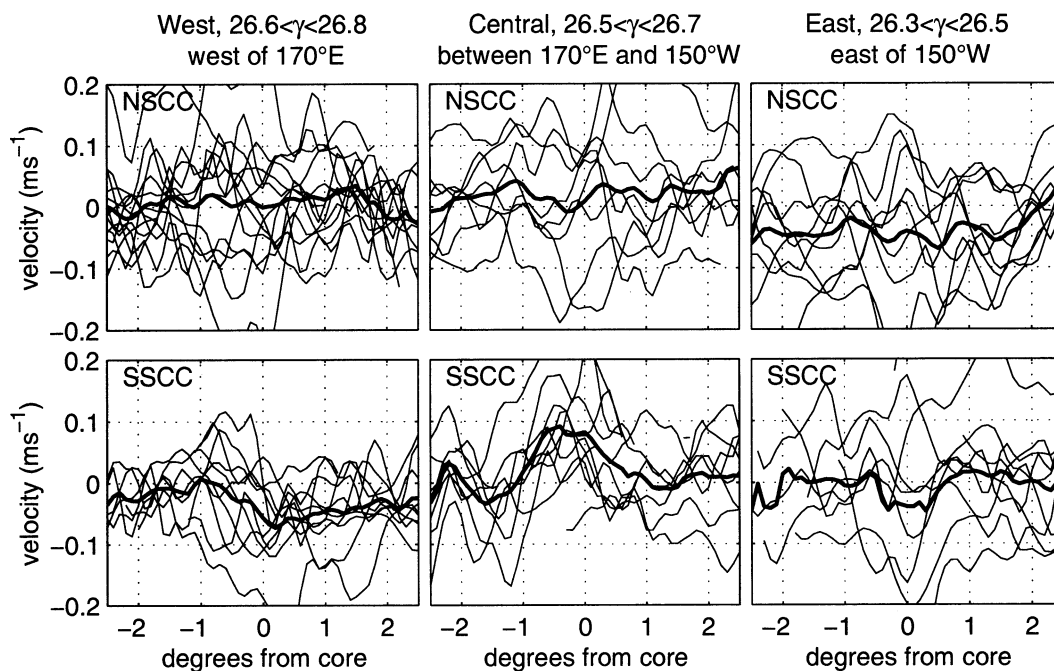

FIG. 7. Observed meridional velocity at core neutral density layers in three longitude regions for the NSCC (upper panels) and SSCC (lower panels). The abcissa in all panels is degrees latitude from the current core, positive to the north. The bold line represents the mean. Observations indicate a highly variable meridional velocity field.
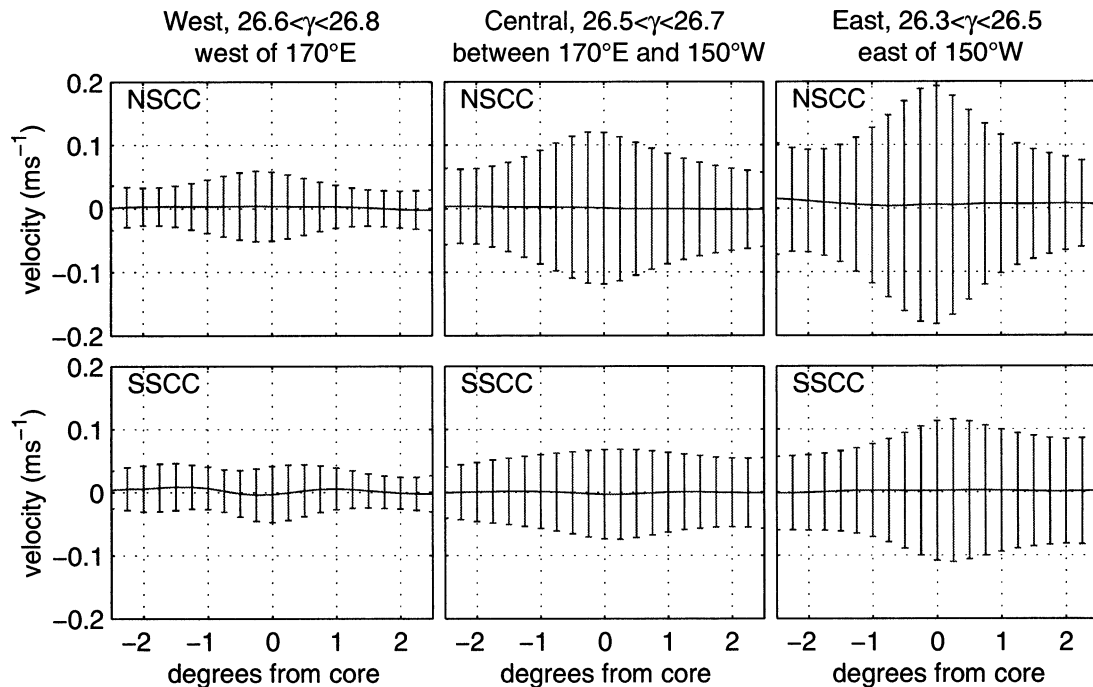
FIG. 8. Model meridional velocity at core neutral density layers averaged in three longitude regions for the NSCC (upper panels) and SSCC (lower panels). The abcissa in all panels is degrees latitude from the current core, positive to the north. The mean is near zero; bars show the standard deviation, not the standard error of the mean.

itude in the eastern Pacific. This change in the sign of the PV gradient indicates the possibility of shear instability. The gradient reversal is caused by the relative PV; planetary PV is nearly constant.

4. Discussion

The ultimate purpose of examining the SCCs in a numerical model and comparing them to observations is to learn something about the SCCs in the ocean; we would like to understand where and how they are forced and dissipated, and how they fit into the general circulation. The question of forcing and dissipation is one on which recent theories differ widely; at one extreme is the zonally independent two-dimensional theory of Marin et al. (2000) and at the other are the three-dimensional theories of Johnson and McPhaden (1999) and MLY. Although we cannot provide definitive critiques of these theories, we can point out some strengths and weaknesses that are indicated by observations and by the JAMSTEC model.

First, however, we address the obvious question of whether the JAMSTEC model represents the SCCs and their associated westward flows better than other comparable global GCMs, and if so, why. Although a detailed comparison is beyond the scope of this note, we have looked at annual mean zonal velocity between 150°E and 100°W from the Parallel Ocean Program (POP: Maltrud et al. 1998), and from the Ocean Circulation and Climate Advanced Modeling (OCCAM)

Project (Webb et al. 1998; Saunders et al. 1999). Representative sections are shown in Fig. 12.

The JAMSTEC model produces the strongest and most realistic SCCs in the annual mean; they are clearly identifiable as isolated maxima at all longitudes. POP produces weaker SCCs, particularly in the western part of the basin, but they are still distinct and identifiable. In OCCAM, the features that most resemble SCCs are even weaker and broader than in POP, and in many sections they appear only as appendages of the equatorial undercurrent or of the north or south equatorial countercurrent. Both JAMSTEC and POP have a sharp equatorial thermocline above a thermostad, but in OCCAM the thermocline is unrealistically thick and the thermostad is absent. In both POP and OCCAM, the SCCs can be identified in individual snapshots less consistently than in JAMSTEC; a stream-coordinate analysis would be difficult at best.

The three models have nearly identical horizontal resolution (JAMSTEC and OCCAM are 0.25°, POP is 0.28° at the equator) but differ in vertical resolution (55 levels in JAMSTEC, 36 levels in OCCAM, and 20 levels in POP), lateral diffusivity (Laplacian in OCCAM, biharmonic in POP and JAMSTEC), and forcing [Hellerman and Rosenstein (1983) in JAMSTEC, monthly average European Centre for Medium-Range Weather Forecasts (ECMWF) winds from 1986 through 1988 in OCCAM, and daily ECMWF winds from 1995 in POP]. The various wind products differ substantially in the equatorial Pacific, so perhaps the relatively strong forc-
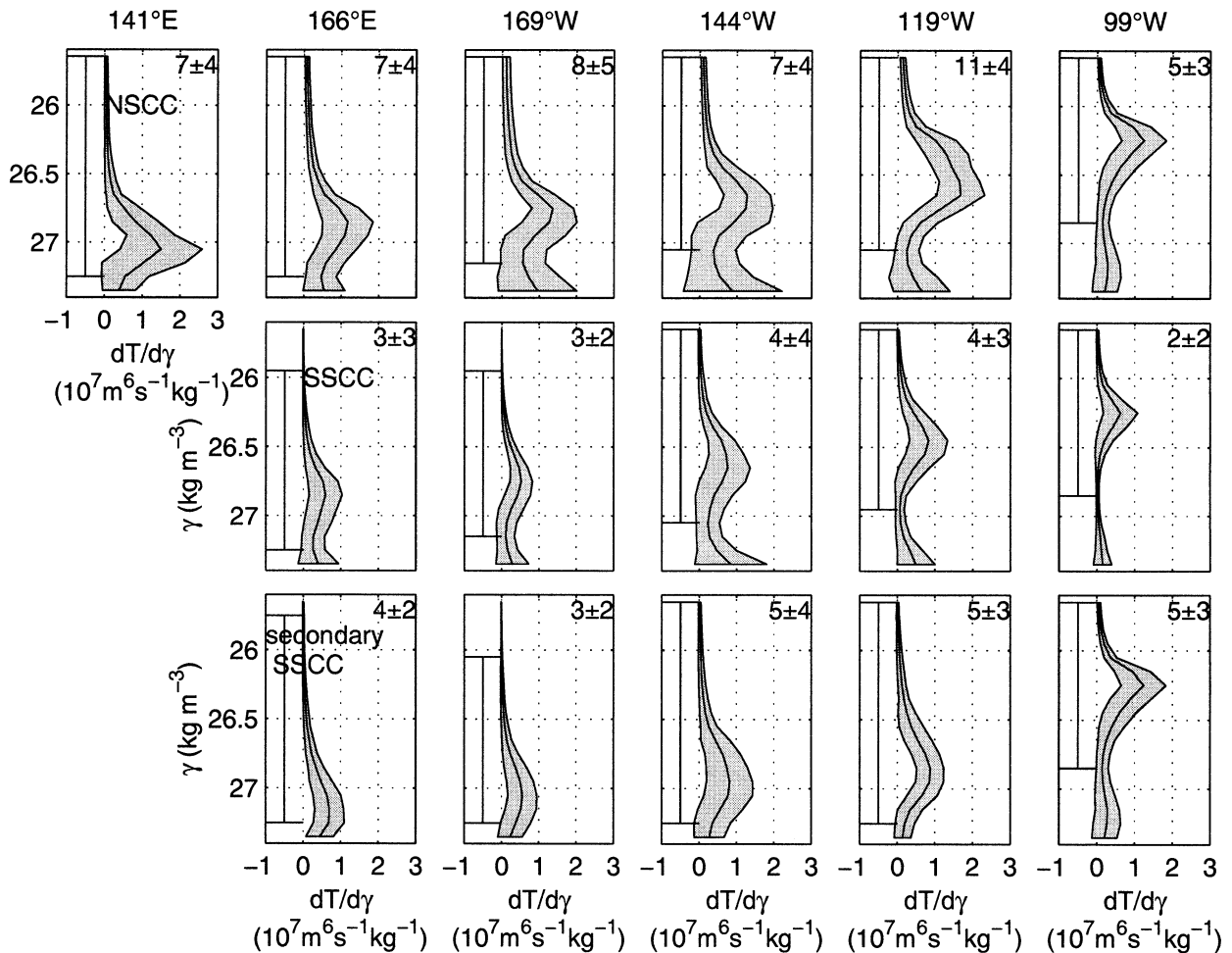
FIG. 9. Model NSCC (upper panels), SSCC (middle panels), and secondary SSCC (lower panels) transport per unit potential density. SCC transport cores progressively lighten as the currents flow across the Pacific. Latitudinal SCC boundaries were estimated for individual neutral layers using the transition from positive to negative neutral-layer velocity when possible; otherwise, the latitude of the local neutral-layer velocity minimum was used. The shading represents one standard deviation. Numbers in the upper right-hand corner of each panel show the mean transport plus/minus the standard deviation (not the standard error) within the density range shown by the vertical line segment to the left.

ing by the Hellerman and Rosenstein (1983) climatology (Harrison 1989) helps the JAMSTEC model produce strong SCCs. We suspect, however, that JAMSTEC's superior vertical resolution is the main reason why it develops more realistic SCCs than POP. If so, then OC-CAM's poor performance is puzzling, but presumably it is related to its thick thermocline and lack of a thermostad. The use of Laplacian lateral diffusivity in OC-CAM may play a role, but it is probably not critical; the thermocline, thermostad, and SCCs in a new 0.125° OCCAM run (not shown) are improved only slightly relative to the 0.25° run.

All three models underestimate the SCC strength more in the western part of the basin than elsewhere. This suggests that in comparison to the ocean they are too dissipative and/or they concentrate too much of their SCC forcing in the east. To the extent that forcing and dissipation are not in balance at each longitude, effects

of any changes in forcing are presumably propagated westward via long Rossby waves as in the theory of MLY. Then in the nondissipative limit the SCC transport at a given longitude would be determined by forcing at longitudes to the east and would be independent of conditions to the west. This is consistent with the inertial theory of Johnson and Moore (1997); although they numerically calculated the SCC shape by integrating eastward from an initial condition in the west, this was an arbitrary choice, and it is physically more reasonable to view their inertial jet as sucked from its eastern end, perhaps by upwelling as in the model of MLY. With the addition of dissipation, the influence of forcing in the east will be gradually damped to the west; if the effective damping (including numerical effects as well as explicit diffusivity) in the numerical models exceeds the damping in the ocean, then SCCs forced in the east would indeed be weaker than observed in the west.
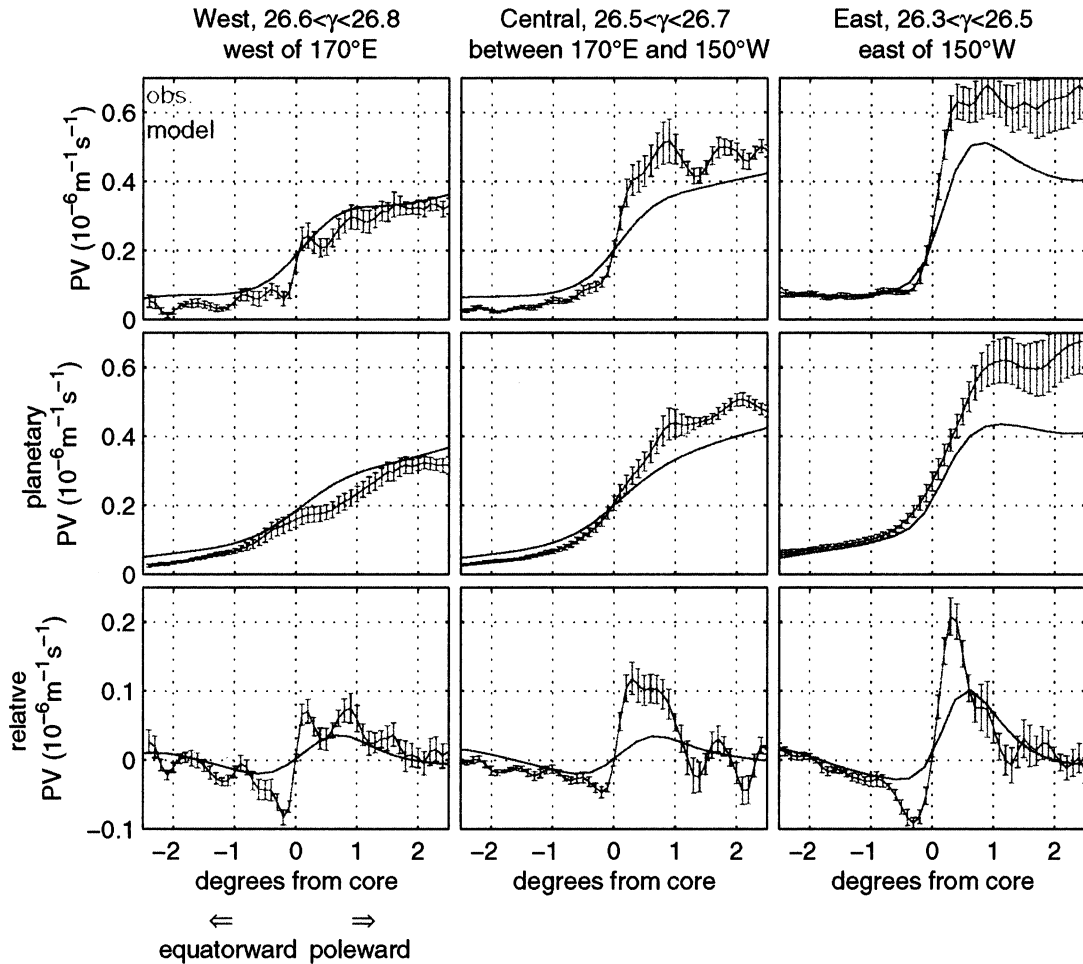
FIG. 10. NSCC PV in core neutral density layers averaged in three longitude ranges for model (blue) and for observations from Rowe et al. (2000) (red). The abcissa in all panels is degrees latitude from the current core, positive to the north. The velocity maximum separates regions of nearly uniform PV: low on the equatorward side, high on the poleward side. Potential vorticity is more uniform on the equatorward side of each NSCC core. Relative vorticity sharpens the PV front at each NSCC core. The PV gradient in the core is much weaker in the model than in observations, and relative vorticity plays only a minor role. The error bars for the observations show one standard error.

Downstream changes in the positions and densities of SCC cores in models and in observations also depend on the zonal distribution of forcing and dissipation. The primary SCC cores in the JAMSTEC model maintain constant latitude from west to east, despite the eastward shoaling of the model thermocline; vertically integrated PV is not conserved. Although this may be viewed as a serious shortcoming of the model, it may also provide a clue about the dynamics of the SCCs: perhaps basinwide PV conservation, the key feature of the Johnson and Moore (1997) model, is not an essential requirement for the formation of SCCs. Potential vorticity conservation may control the downstream shift of the core latitude, however.

The downstream lightening of the cores in the model and in the ocean may be more important, however. In isopycnal coordinates, the lightening is seen clearly as zonal divergence above the jet core and zonal conver-gence below it; that is, the eastward velocity increases to the east in the upper part of the jet and decreases to the east in the lower part. Mass conservation requires that any such zonal divergence (taking the upper part of the jet as an example) be balanced by net convergence in the vertical–meridional plane, but the relative im-portance of isopycnal meridional convergence versus diapycnal vertical convergence is not obvious. In the limit of no meridional convergence, water flowing east within the jet would be lightened entirely by diapycnal mixing, with a buoyancy flux into the top of the jet exceeding the flux out the bottom. This would occur with constant diapycnal diffusivity because the density gradient is stronger at the top of the SCCs than at the bottom. Conversely, if diapycnal mixing is negligible, then the jet must lighten downstream via isopycnal cir-culation, with meridional convergence above the core and divergence below. This appears to be the dominant
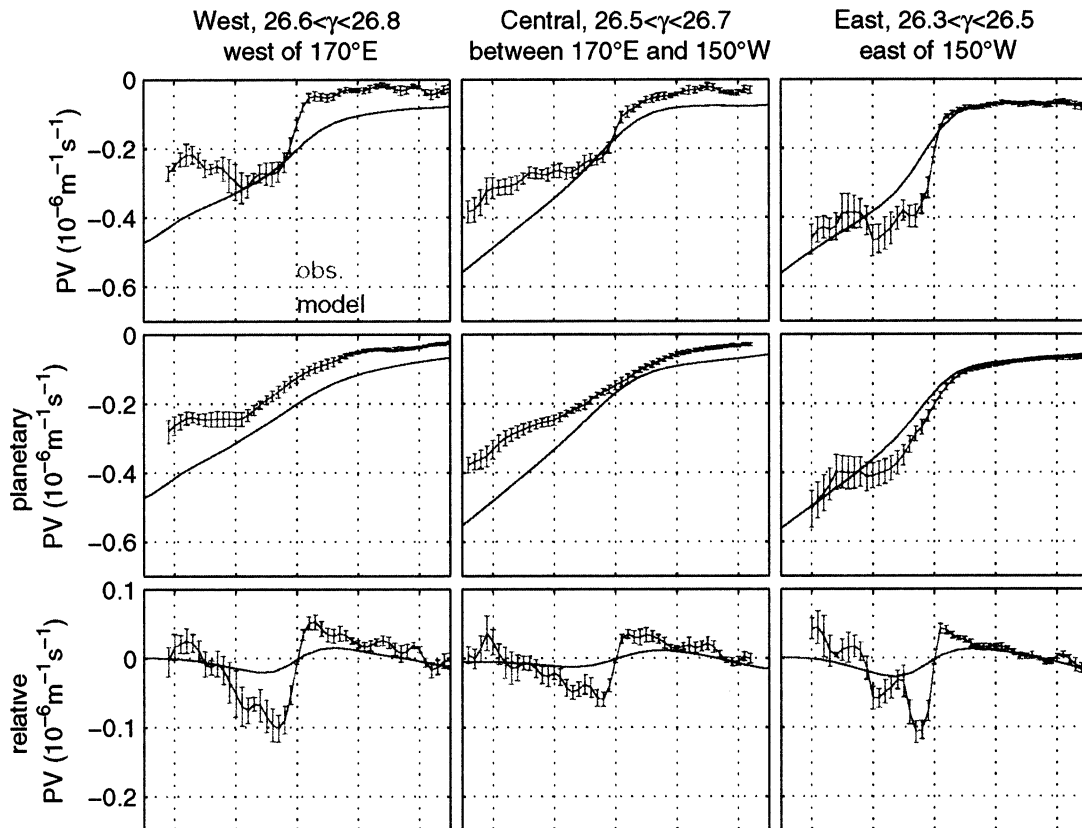
FIG. 11. Same as Fig. 10 but for the SSCC. Pools of nearly uniform low PV are found on the equatorward side of the model SSCCs, as observed. Regions of uniform high PV on the poleward side of the SSCC shown in observations from Rowe et al. (2000) are not present in the model; magnitude of PV continues to increase through the jet core and poleward flanks.

process in the JAMSTEC model, as described in detail by Ishida et al. (2001, unpublished manuscript). We are aware of no dataset that would allow the processes to be quantified in the ocean. A scale calculation indicates the difficulty of the task, even when working with numerical model output. Suppose the flow were entirely isopycnal. Within a layer that is in the core in the west, but is nearly at rest in the east, the zonal velocity drops from 20 cm s^{-1} to zero in a distance of order 10 000 km; if the meridional scale of the jet is 100 km, a meridional velocity component of only 0.2 cm s^{-1} in magnitude, diverging from the core, balances the zonal convergence of the zonal velocity component. If the meridional divergence were zero, then the zonal convergence would be balanced by a divergent vertical velocity difference of 2×10^{-4} cm s^{-1} over 100 m. Direct observational support for either vertical or meridional divergence will be very difficult to obtain.

The two-dimensional model of Marin et al. (2000) has some features in accord with observations, but it also has shortcomings apart from its lack of zonal structure. It produces a meridional profile of jet velocity that is sharply peaked at the core, as in observations (Rowe et al. 2000) and to a lesser extent in the JAMSTEC

model. The mean circulation in the Marin et al. (2000) model includes meridional overturning cells (Hadley cell analogs) driven by relaxation of the density field to a uniformly sloping mean thermocline. It is not clear that this rather unphysical forcing corresponds to any physical process in the JAMSTEC model or in the ocean. Furthermore, the magnitude of the meridional velocity component in the overturning cells, "$v \sim 4$ cm s^{-1}," is substantially larger than the 0.5 cm s^{-1} or less that we estimate from the JAMSTEC model.
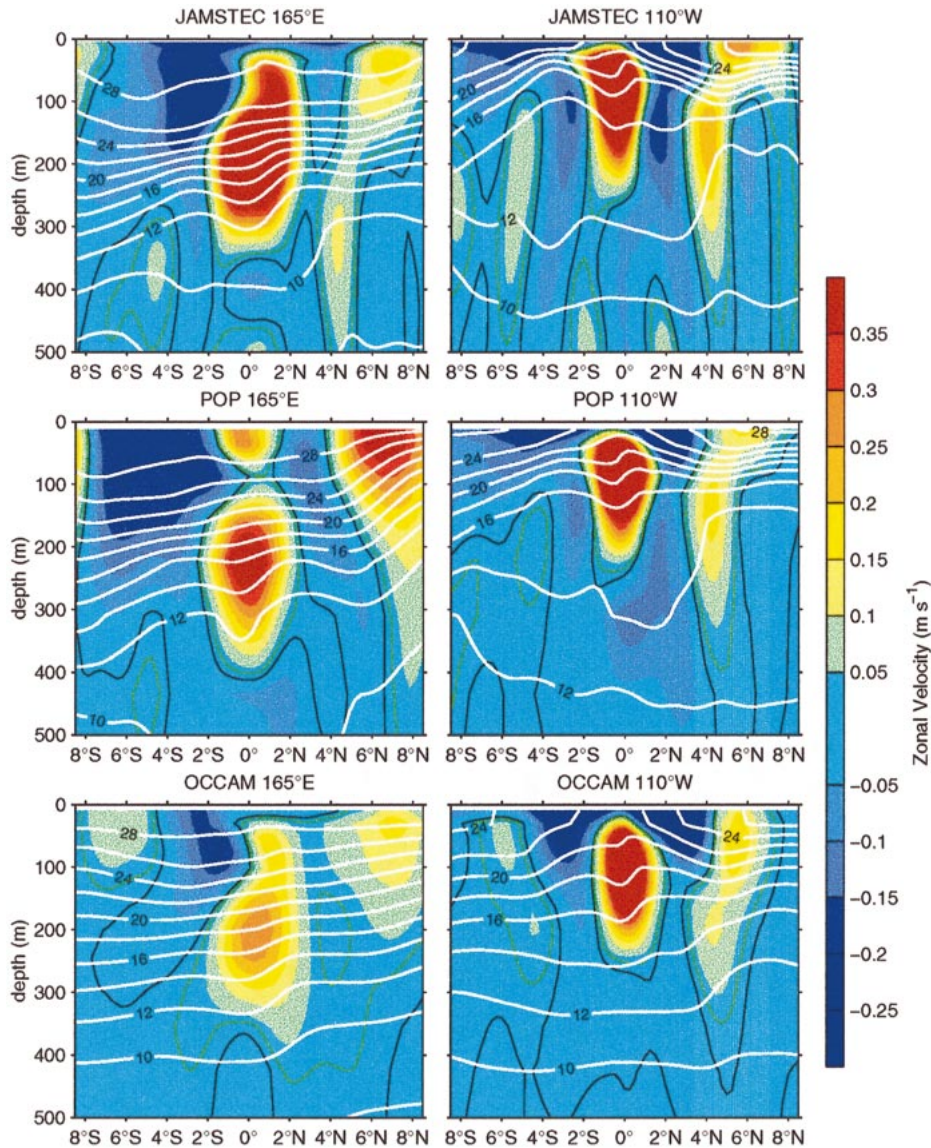
FIG. 12. Annual mean zonal velocity from three global general circulation models: JAMSTEC (top); POP, 1995 (middle); and OCCAM (bottom). The zero zonal velocity contour is black; a green contour is added at 2 cm s^{-1}. Colors change every 5 cm s^{-1}. Potential temperature contours are white lines. The JAMSTEC model produces the strongest and most realistic SCCs. In the west (left panels), the SCCs are badly underestimated by POP and nearly absent from OCCAM.

REFERENCES

Harrison, D. E., 1989: On climatological monthly mean wind stress and wind stress curl fields over the world ocean. *J. Climate,* **2,** 57–70.

Hellerman, S., and M. Rosenstein, 1983: Normal monthly wind stress over the world ocean with error estimates. *J. Phys. Oceanogr.,* **13,** 1093–1104.

Ishida, A., Y. Kashino, H. Mitsudera, and T. Kadokura, 1998a: Mean circulation and variability in the global high-resolution GCM— The equatorial currents system in the Pacific Ocean. *Proc. Int.*

Symp. Triangle '98, Kyoto, Japan, Japan Marine Science and Technology Center, Frontier Research System for Global Change, and International Pacific Research Center, 178–189.

——, ——, ——, N. Yosioka, and T. Kadokura, 1998b: Preliminary results of a global high-resolution GCM Experiment. *J. Fac. Sci. Hokkaido Univ. Ser. 7,* **11,** 441–460.

Jackett, D. R., and T. J. McDougall, 1997: A neutral density variable for the world's oceans. *J. Phys. Oceanogr.,* **27,** 237–263.

Johnson, G. C., and D. W. Moore, 1997: The Pacific Subsurface Countercurrents in an inertial model. *J. Phys. Oceanogr.,* **27,** 2448–2459.

——, and M. McPhaden, 1999: Interior pycnocline flow from the subtropical to equatorial Pacific Ocean. *J. Phys. Oceanogr.,* **29,** 3073–3089.

Levitus, S., 1982: *Climatological Atlas of the World Ocean.* NOAA Professional Paper 13, 173 pp. and 17 microfiche.

Maltrud, M. E., R. Smith, A. Semtner, and R. Malone, 1998: Global eddy-resolving ocean simulations driven by 1985–1995 atmospheric winds. *J. Geophys. Res.,* **103,** 30 825–30 854.

Marin, F., B. L. Hua, and S. Wacongne, 2000: The equatorial thermostad and subsurface countercurrents in the light of atmospheric Hadley cells dynamics. *J. Mar. Res.,* **58,** 405–437.

McCreary, J. P., P. Lu, and Z. Yu, 2002: Dynamics of the Pacific subsurface countercurrents. *J. Phys. Oceanogr.*, in press.

McPhaden, M. J., and Coauthors, 1998: The Tropical Ocean–Global Atmosphere observing system: A decade of progress. *J. Geophys. Res.,* **103,** 14 169–14 240.

Pacanowski, R., 1995: MOM2 documentation user's guide and reference manual. Tech. Rep. 3, Geophysical Fluid Dynamics Laboratory, Princeton, NJ, 232 pp.

——, and S. Philander, 1981: Parameterization of vertical mixing in numerical models of tropical oceans. *J. Phys. Oceanogr.,* **11,** 1443–1451.

Rowe, G. D., E. Firing, and G. C. Johnson, 2000: Pacific Equatorial Subsurface Countercurrents' velocity, transport, and potential vorticity. *J. Phys. Oceanogr.,* **30,** 1172–1187.

Saunders, P., A. C. Coward, and B. A. deCuevas, 1999: Circulation of the Pacific Ocean seen in a global ocean model (OCCAM). *J. Geophys. Res.,* **104,** 18 281–18 299.

Schott, F., and C. Böning, 1991: The WOCE model in the western equatorial Atlantic: Upper layer circulation. *J. Geophys. Res.,* **96,** 6993–7004.

Tsuchiya, M., 1975: Subsurface countercurrents in the eastern equatorial Pacific Ocean. *J. Mar. Res.,* **33,** 145–175.

Webb, D. J., B. A. de Cuevas, and A. C. Coward, 1998: The first main run of the OCCAM global ocean model. Internal Rep. of James Rennell Division, SOC Tech. Rep., Southampton Oceanography Centre, Southampton, United Kingdom, 44 pp.